Configurational Polytopes Near the Jamming Limit

Frank H. Stillinger, Chemistry Dept., Princeton University

4-12-07

Figure 0. Lecture title, workshop title and dates, principal collaborators.

Hard particle models for many-body systems possess several important virtues. Ease of visualization for allowed configurations is certainly one. Another is that they represent an extreme limit of anharmonicity for dense forms of matter. Beyond those features, they have an economical mathematical definition, while nevertheless exhibiting complex and fascinating phenomena. Explanations of those phenomena in many cases remain incomplete or even missing, and so provide irresistible challenges for theorists. This lecture focuses on some aspects of hard-particle models in their nearly-jammed states, both ordered and disordered. Limited time will impose restriction to the simplest of hard-particle models: monodisperse rods, disks, and spheres, in d = 1, 2, and 3 Euclidean dimensions respectively. Figure 1 provides the starting point.

Figure 1. Elementary hard particle models.

The general situation to be described involves N identical rods, disks, or spheres in a container with fixed size and shape to which periodic boundary conditions apply. Furthermore, for a given container size the common particle diameter a can be chosen large enough so that the particles become trapped by their non-overlap constraints. Each of the N particles then will be narrowly confined by the presence of its immediate neighbors that themselves are similarly narrowly confined. Independent small particle displacements remain possible in such a trapped state until increase in the particle diameter gives rise to particle jamming, say at $a = a^*$, at which permanent neighbor contacts exist and only the overall translational motion permitted by periodic boundary conditions is possible.

Three distinct jamming categories at $a = a^*$ deserve to be distinguished. These are briefly defined in Figure 2, where they are listed in order of increasing stringency. For the purposes of this lecture,

---

Figure 2. Three jamming categories.

---

it is the second of these that will be required. Barring overall system translation, no non-overlap collective (simultaneous) motion of any subset of particles will be possible allowing the system ultimately to escape from the neighborhood of jamming. Of course this requirement will also include strictly jammed cases as well. Figure 3 provides an obvious illustrative example in two dimensions for

---

Figure 3. Collectively (and strictly) jammed disk state, $N = 39$.

---

collectively jammed disks. It belongs to the family of triangular crystals that can contain irregular arrangements of monovacancies while still fulfilling at least the "collectively jammed" requirement.

Indeed the specific example shown in Figure 3 is both collectively jammed as well as strictly jammed. We will also consider amorphous (irregular) packings that are collectively jammed. An example for spheres is shown in Figure 4.

Figure 4. Amorphous sphere packing, $N = 500$, $\varphi = 0.64$ [Donev, et al., J. Appl. Phys. 95, 989-999, (2004), Fig. 5].

Figure 5 raises the minor technical issue of "rattlers". These are particles in 2 and 3 dimensional

---

Figure 5. Four disk rattlers, $N = 250$ [Donev, et al., J. Appl. Phys. 95, 989-999 (2004), Fig. 9].

---

disk and sphere packings that even in the system-jammed state are not themselves jammed by neighbors, but only loosely confined within a prison of jammed neighbors. The example shown, presenting the unit cell and three images, has each of the four rattlers confined by a convex heptagon of neighbors. In various irregular packing preparations of disks and spheres, these rattlers have been found to comprise up to several percent of the N particles. Formally these configurations would not fall into any of the three jamming categories defined in Figure 2. However, we will simply suppose that any rattlers have been removed, and so we will confine attention just to the jammed network of the remaining majority. N will now stand for only those particles remaining after rattler removal.

Figure 6 presents the current estimates of the covering fraction ranges over which collectively jammed configurations can exist in $d = 1,2,$ and 3 dimensions.

Figure 6. Covering fraction ranges for collectively jammed rods, disks, and spheres.

A basic message of this lecture concerns the value of examining the geometry of the available portion of multidimensional configuration space for the N-particle system as a whole, *i.e.* that portion free of particle overlap. Under the periodic boundary condition convention it is natural to hold the system centroid fixed, so the dimension of the relevant subset of configuration space is $D = (N-1)d$ for N particles. When the particle diameter a is sufficiently small, the accessible portion of that space is singly connected (for $d > 1$). But as the diameter increases (increasing covering fraction φ) the system experiences configurational disconnections, leaving local "jamming" regions that eventually disappear upon further particle size increase (equivalent to compression). In the elementary rigid rod case, disconnection applies at all densities on account of the fact that impenetrable rods cannot pass one another on the line.

Figure 7 schematically indicates the basic properties of a trapping region in configuration space,

---

Figure 7. Trapping region in $D = (N-1)d$ -dimensional configuration space.

---

determined by non-overlap constraints. These overlap constraints take the form of hypersurfaces, specifically hypercylinders for $d > 1$, one for each pair of particles that can come into contact. At the center of such a trapping region is the location $\mathbf{r}_1^*,...,\mathbf{r}_N^*$ of the jammed particle configuration. This is identified by growth of the diameter a to its local maximum a^*. Of course there are equivalent small regions elsewhere in the multidimensional configuration space corresponding to the other $(N-1)!-1$ particle permutations that cannot be attained by system translations permitted by the periodic boundary conditions. Additionally there can be other non-equivalent disconnected, nearly jammed, regions (indexed by l) whose own jamming diameters a_l^* are close to that of the region under consideration.

The disconnection phenomenon obviously implies loss of ergodicity for the *N*-particles as a dynamical system.

Upon approach to the jamming limit $a = a*$ for the specific disconnected region of interest, the linear dimensions of the available region shrink monotonically to zero. Consequently hypersurface curvature ($d = 2,3$) becomes asymptotically irrelevant. This means that asymptotically the hypercylinders can be replaced by tangent hyperplanes. Thus the limiting shape of the local allowed configuration space region is a convex "polytope". Figure 8 outlines this replacement and its immediate

---
Figure 8. Hyperplane selection and resulting convex polytope.
---

consequences. Geometric properties of these polytopes and their many-body-phenomenon implications form the subject of this lecture. The value of this multidimensional approach and the polytopes it identifies for hard-particle systems was first identified 45 years ago by Salsburg and Wood. Their pioneering paper is indicated in the next Figure 9, along with a few other literature references that

---
Figure 9. Relevant publications.
---

are relevant to polytope geometry and hard-particle statistical mechanics.

One of the basic polytope properties is a generalized Euler theorem, Figure 10. This is familiar in

---
Figure 10. Generalized Euler's theorem; result for simplices.
---

its three-dimensional version, stating a linear equality that is satisfied by the numbers of faces (*f*), edges (*e*), and vertices (*v*) of any polyhedron. The generalization to arbitrary dimension *D* requires enumeration of j-dimensional "j-faces". In our present context these are the mutual intersections of $D - j$ pair-contact tangent hyperplanes [*i.e.* the $(D-1)$-faces].

The *j*-face enumeration is straightforward for simplices, the polytope type relevant to the rigid rod case, because pair contacts occur substantially independently of one another. This implies that all of the simplex $(D-1)$-faces are equivalent in size and shape for rigid rods. However for disks and spheres the enumeration generally is not straightforward. As Figure 11 illustrates pair contacts do not always occur

---
Figure 11. Pair contacts surrounding a central disk.
---

independently, but the existence of some pair contacts can automatically force others into contact as well. When applicable, this local crowding phenomenon implies that the total count of j-faces for all $0 \le j \le D-1$ will be less than that for a simplex in the same number of dimensions *D*.

A basic problem obviously is finding the content Ω of the polytopes. In terms of earlier notation, this amounts to the evaluation of the multiplier *C* in the expression $\Omega = C(a*-a)^{(N-1)d}$. Unfortunately there is no generally useful procedure for doing this when *N* is large. However the result is known for regular simplices in arbitrary dimension. This includes the case of the rigid-rod polytope, with results outlined in Figure 12. For this relatively straightforward example it is worth noting that the

---
Figure 12. Rigid rod system: Regular simplex in arbitrary dimension.
---

contents of the inscribed and circumscribed hyperspheres, formally giving lower and upper bounds for Ω, are thermodynamically useless. However, a simple "independent cell" approximation produces a thermodynamically relevant, but crude lower bound. This approximation limits each rod to displacements about the regular periodic arrangement with maximum displacement small enough so as not to restrict similar displacements of its two neighbors.

These bounding relationships extend to the more general cases for disk and sphere system limiting polytopes. For large *N* these polytopes are highly protuberant, shapes that again cannot be adequately approximated by inscribed or circumscribed hyperspheres. But at least for regular packings, the cell method qualitatively captures polytope protuberance, and yields a thermodynamically relevant, though crude, lower bound to the polytope content. It is illustrated graphically in Figure 13 for a disk crystal. However, finding analytic procedures to calculate the polytope content exactly, or even just with high

---
Figure 13. Independent displacement cells for a disk crystal.
---

numerical precision, remains generally unsolved. Of course MC and MD computer simulations for finite *N*, (a) with density integration from the ideal gas limit, or (b) "tether" methods, provide good estimates of the exact infinite-system-limit results. In principle the crude independent-cell estimate can also be adapted to irregular packings, given the jammed configuration $\mathbf{r}_1 *...\mathbf{r}_N *$.

It is worth noting that another procedure, due to Zevi Salsburg [J. Chem. Phys. **44**, 3752 (1966)], generates a thermodynamically relevant upper bound on polytope content for the triangular disk crystal and the face-centered cubic sphere crystal, as each approaches its jamming limit. The method involves including only those neighbor interactions along two of the three neighbor directions for the disk crystal, and along three of the six neighbor directions in the fcc sphere crystal. This amounts to removing sets of faces from the true polytope, and extending those that remain until they produce closure. By counting the number of remaining hyperfaces, one realizes that this constructs a circumscribed simplex for the disk or sphere polytope. The resulting simplex has lower symmetry than that for the rigid rod system in the same number of dimensions. However, Salsburg has shown that its content can be obtained from the fact that these modified many-particle systems amount to two or three independent rigid rod systems, in the cases of disks and spheres respectively.

The next aspect of the configurational polytope analysis to be considered is the distribution of particle pairs. For any one of those pairs that contribute hyperplane-faces to the limiting polytope, the probability distribution of their separation beyond contact is simply given by the polytope's cross-sectional hyper-area generated by a hyperplane sweeping across the polytope, parallel to the hyperface, toward the far extreme. This is schematically illustrated in Figure 14. The distance distribution for

---
Figure 14. Polytope cross section determining particle pair distance separation.
---

these pairs thus starts with a discontinuity at contact. For other (non-contacting) pairs the relevant cross sectioning hyperplanes are not parallel to a hyperface, and thus their distance distributions rise continuously from zero.

Polytope hyperfaces, the $[(N-1)d-1]$-dimensional faces that were selected as tangent hyperplanes to the original hypercylindrical surfaces, are perpendicular to one another if the generating contact pairs have no particle in common. However they are not perpendicular if there is a common particle. One finds that the angles of these particle-sharing cases are always $\leq 2\pi/3$. [Figure?] These angles are directly relevant to the initial-slope behavior of distance distributions for contacting pairs.

Because we are concerned with the asymptotic approach to a collectively jammed configuration, a state at which particle displacements become zero, coordinate rescaling becomes natural. Recalling that linear dimensions of the polytope behave in that limit as $a*-a$, Figure 15 provides the scale change.

Figure 15. Jamming-limit scale change for distances.

The Brünn-Minkowski inequality for convex polytopes, Figure 16, guarantees that each of these pair

---
Figure 16. Brünn-Minkowski inequality.
---

separation distributions can individually possess only a single maximum as a function of distance.

Joint probabilities for two or more pairs are proportional to the measure of the intersection of the respective hyperplanes within the polytope. These joint probabilities may or may not involve pairs that share a particle.

The polytope is a simplex not only for the rigid rod case, but also a large class of irregular (amorphous) jammed packings of disks and spheres. These are often termed "isostatic" packings. The next Figure 17 examines the contacting-neighbor pair separation probabilities for these simplex cases.

Figure 17. Contacting-pair distance distribution for simplex polytope cases.

A convenient simplification occurs. The cross sections parallel to the hyperfaces remain strictly similar in shape to the hyperface, and scale uniformly in size with a power given by dimension $D = (N-1)d-1$ as the single remote vertex (f_0) is approached. In the large system limit of primary interest here, this amounts to an exponentially damped distance distribution. Obviously all neighbor pairs in the rod system are identical and so have identical exponential decay rates. But that is not the case for irregular isostatic packings of disks and spheres.

Figure 18 considers the isostatic amorphous packing situation (disks and spheres) in further detail.

Figure 18. Simplex geometry and distance distributions for amorphous packings of disks and spheres.

The limiting simplex polytopes have low symmetry, or perhaps even no symmetry. The hyperfaces (themselves simplexes) will exhibit a distribution of hyperareas. It is important to note that the displacement distance that a cross section must travel across the polytope is inversely proportional to the area, and this translates into an inverse proportionality to the (large-system) exponential decay rate of the distance distribution function for that pair. The net averaged pair distribution function for contacting pairs thus is an average over all exponential decays present. Although the result is non-exponential, it nevertheless has its maximum at contact and is monotonically declining with separation, consistent with the Brünn-Minkowski theorem implication.

A disk or sphere system confined to a polytope is dynamically an ergodic system. That is, energy-conserving Newtonian dynamics with elastic collisions between pairs of particles eventually uniformly samples the polytope interior and uniformly distributes collisions over all hyperfaces. The collision rate for any contacting pair will thus be proportional to its hyperface hyperarea. The collision rate can be interpreted as a time-averaged repulsive force acting between the pair. Figure 19 presents a distribution

---
Figure 19. Force distribution, $N = 1000$ and 10,000 hard spheres, amorphous packing [Donev, et al., Phys. Rev. E 71, 011105 (2005), Fig. 7].
---

of area (as a force distribution) for large hard sphere irregular collectively jammed packings. This and similar results suggest that the force distribution remains positive down to vanishing hyperface hyperarea, at least for spheres in amorphous packings. By implication there are many hyperplanes

lurking just outside the limiting polytope, and these would begin to contribute new bounding surfaces to the available configuration space for the *N*-particle system as the collision diameter *a* is slightly reduced. This is confirmed by examining the conventional pair correlation function for spheres in an amorphous packing, an example of which appears in Figure 20. This representative case clearly displays a buildup

---

Figure 20. $g(r)$ for five amorphous sphere packings, N=10,000 [Donev, et al., Phys. Pev. E 71, 011105 (2005), Fig. 9].

---

of pair distances in the jammed state just beyond contact, that is, just beyond those (a Dirac delta function in this representation) providing simplex hyperfaces. The effect of these near-contact pairs on the system's pressure is a positive contribution, beyond what mere expansion of the polytope region would be with density reduction.

Leaving aside the irregular amorphous packings, consider next the case of the face-centered cubic sphere packing. This is one of the maximum-density arrangements (along with hcp and the interpolating hybrid stackings). It consists of four interpenetrating simple cubic sublattices. Upon removal of any or all of the spheres from one of those four sublattices, this remains not only collectively jammed but also strictly jammed. As spheres are removed from the one sublattice, the average number of contacts per remaining particle declines from 12 to 8. This changes the polytope to a more protuberant form, moving it partially toward simplex character. It is interesting to see how the average pair separation for contacting pairs evolves as the one sublattice is randomly vacated. Figure 21 shows what happens. The

---

Figure 21. Evolution of contact-neighbor peak as one sublattice is randomly vacated; initial system contained $N = 13500$ spheres [Donev, et al., Phys. Rev. E 71, 011105 (2005), Fig. 11].

---

peak initially beyond contact moves inward and develops into a monotonically decreasing function of distance. In periodic structures, larger numbers of nearest neighbors have the effect of localizing the distance distribution away from contact. This can be observed in a fixed dimension as in this example, or as dimension increases with corresponding "kissing number" increase.

The last aspect of this polytope analysis to be examined concerns elastic behavior of the nearly-jammed system. Normally this would require the container shape be deformed, and specifically would demand that the packing involved be strictly jammed. But if the system is large, elastic constants can be extracted from the polytope moment tensor. This will now be demonstrated for structurally perfect periodic crystals: disks in a triangular crystal, spheres in an fcc or hcp crystal. As shown in the next Figure 22, the moment tensor for the corresponding polytope is defined in terms of reduced

---

Figure 22. Definition of the polytope moment tensor in terms of reduced displacements $\mathbf{t}_j$.

---

displacement vectors for the *N* particles, in the fixed centroid subspace.

Figure 23. Isothermal elastic constants.

Apparently the geometric reason that elastic constants can be extracted from properties of the undisplaced system is relatively simple. Uniform distortion of the system principally affects the outer protruding portions of the polytope. Analogously the moment tensor also is dominated by those outer portions.

In reaching the end of formal remarks, it's worth emphasizing that a substantial list of unsolved problems still face us. Some are listed in the last Figure X, whose answers are desirable objectives.

Figure X. Some unsolved problems.

---

for further research. This foreshortened list only includes monodisperse disk and sphere systems, but it should be obvious that generalizations to mixtures, rigid non-spherical particles, and systems in more than three dimensions also offer challenging opportunities.

~~~~~
~~~~~

BACK

Configurational Polytopes Near the Jamming Limit

[A lecture delivered at the Princeton Center for Theoretical Physics workshop "Packing Problems, Classical Ground States, and Glasses", April 12-13, 2007.]

Frank H. Stillinger
Department of Chemistry,
Princeton University, Princeton, NJ 08544

Principal collaborators:

Edmund A. DiMarzio
Zevi W. Salsburg
Boris D. Lubachevsky
Ronald L. Graham
Salvatore Torquato
Aleksandar Donev
Robert Connelly

BACK

Elementary Hard Particle Models

- Monodisperse rigid rods ($d=1$), rigid disks ($d=2$), rigid spheres ($d=3$).
- N particles in fixed container, with periodic boundary conditions.
- Collision diameter $a>0$ to be treated as adjustable.
- Maximum attainable densities (ρ) and covering fractions (φ):

  rods: $(\rho a)_{\max}=1, \quad \varphi_{\max}=1$;

  disks: $(\rho a^2)_{\max}=2/3^{1/2}, \quad \varphi_{\max}=\pi/(2\cdot 3^{1/2})$;

  spheres: $(\rho a^3)_{\max}=2^{1/2}, \quad \varphi_{\max}=\pi/(2^{1/2}\cdot 3)$.

- Disk and sphere systems exhibit arrays of jammed structures, both regular and irregular geometrically, with non-trivial ranges of ρa^2 or ρa^3 values.

BACK

Disk and Sphere Jamming Categories

[arranged by increasing stringency]

Locally jammed: On account of neighbor contacts, no particle can be individually displaced.

Collectively jammed: No subset of particles can be simultaneously displaced allowing subsequent motions of all particles that would eliminate every contact.

Strictly jammed: Collectively jammed configuration that resists all possible uniform container shear strains.

Princeton Lecture
April 12, 2007
F.H. Stillinger
Figure 3

BACK

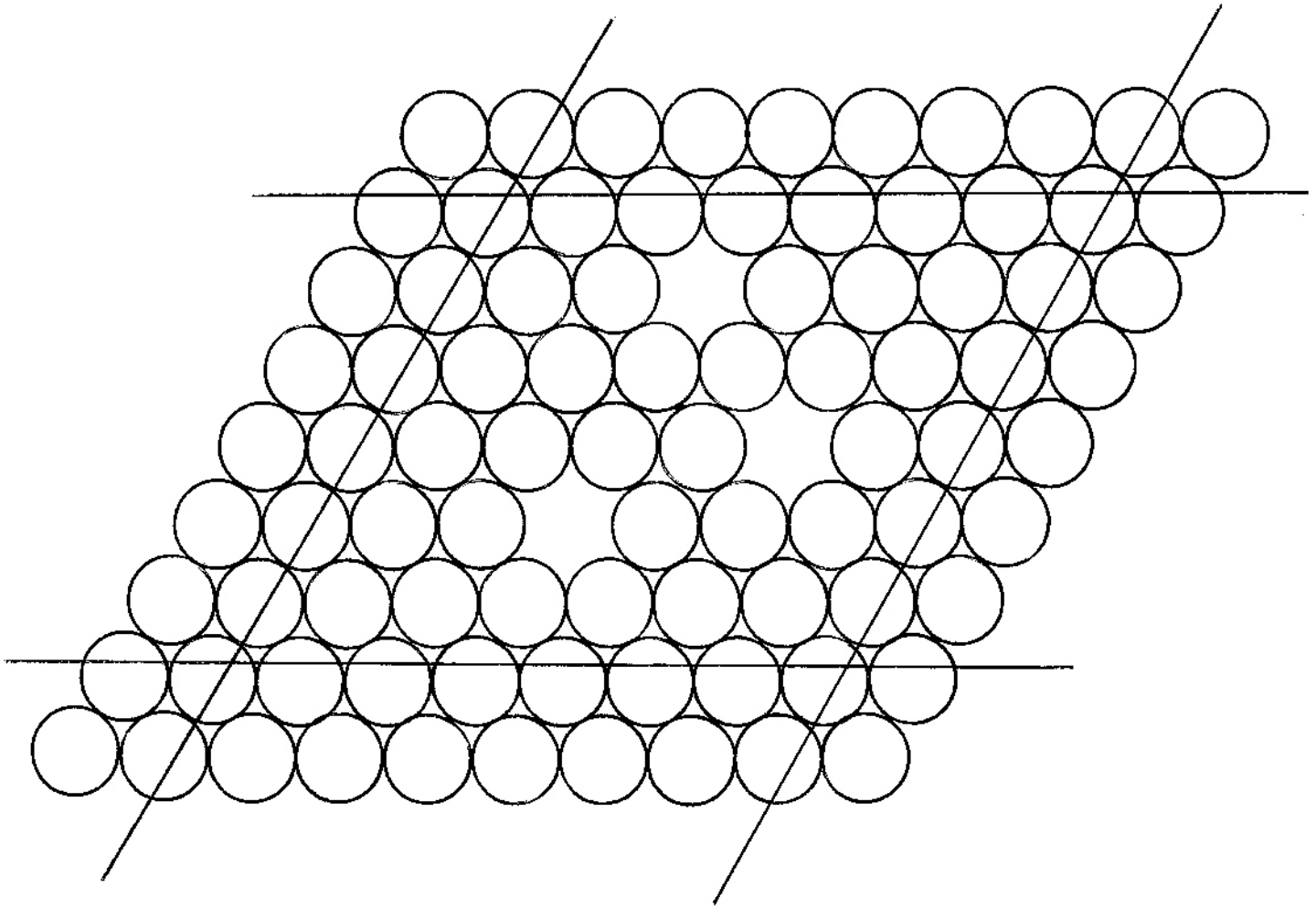

Princeton Lecture
April 12, 2007
F.H. Stillinger
Figure 4

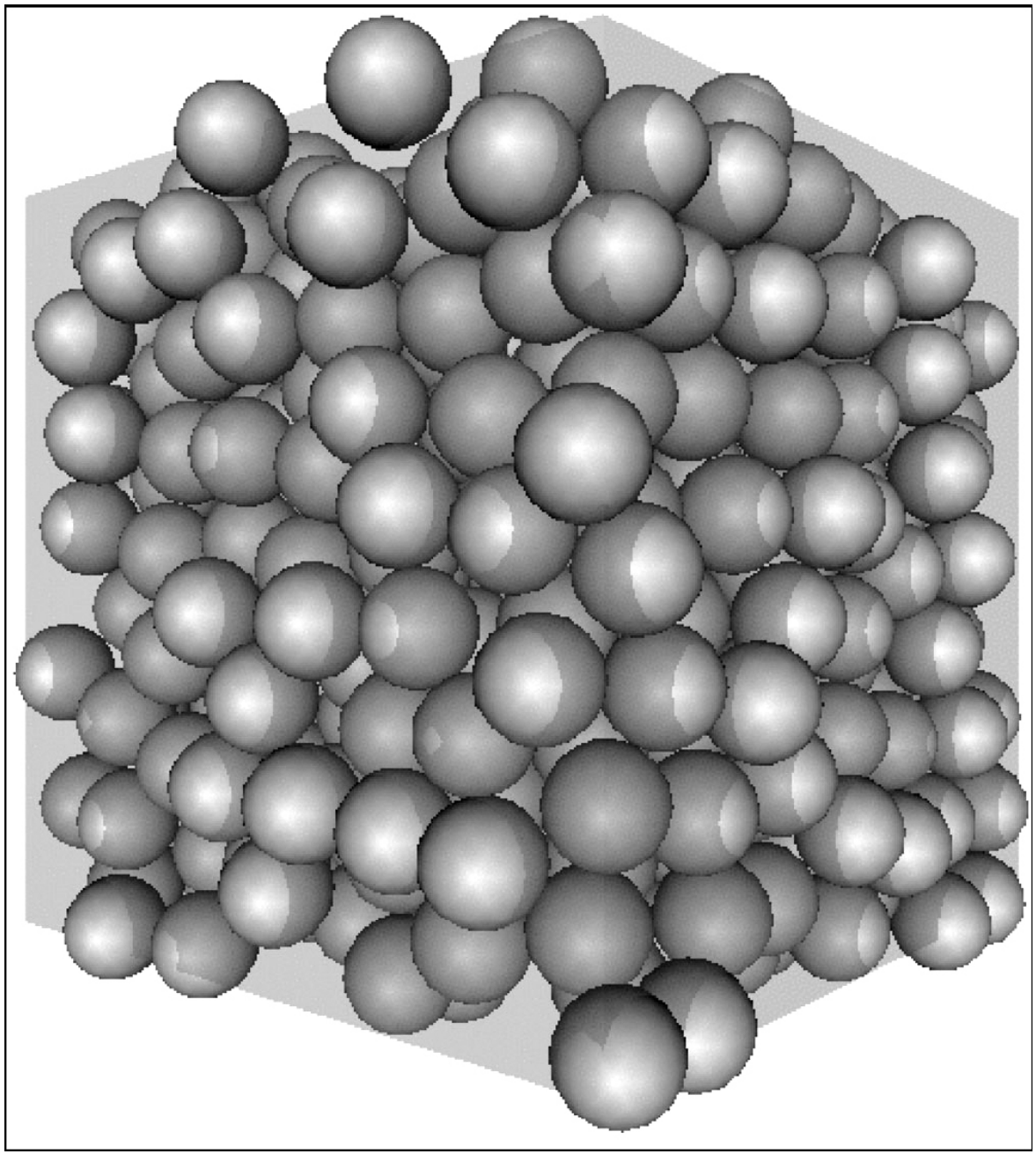

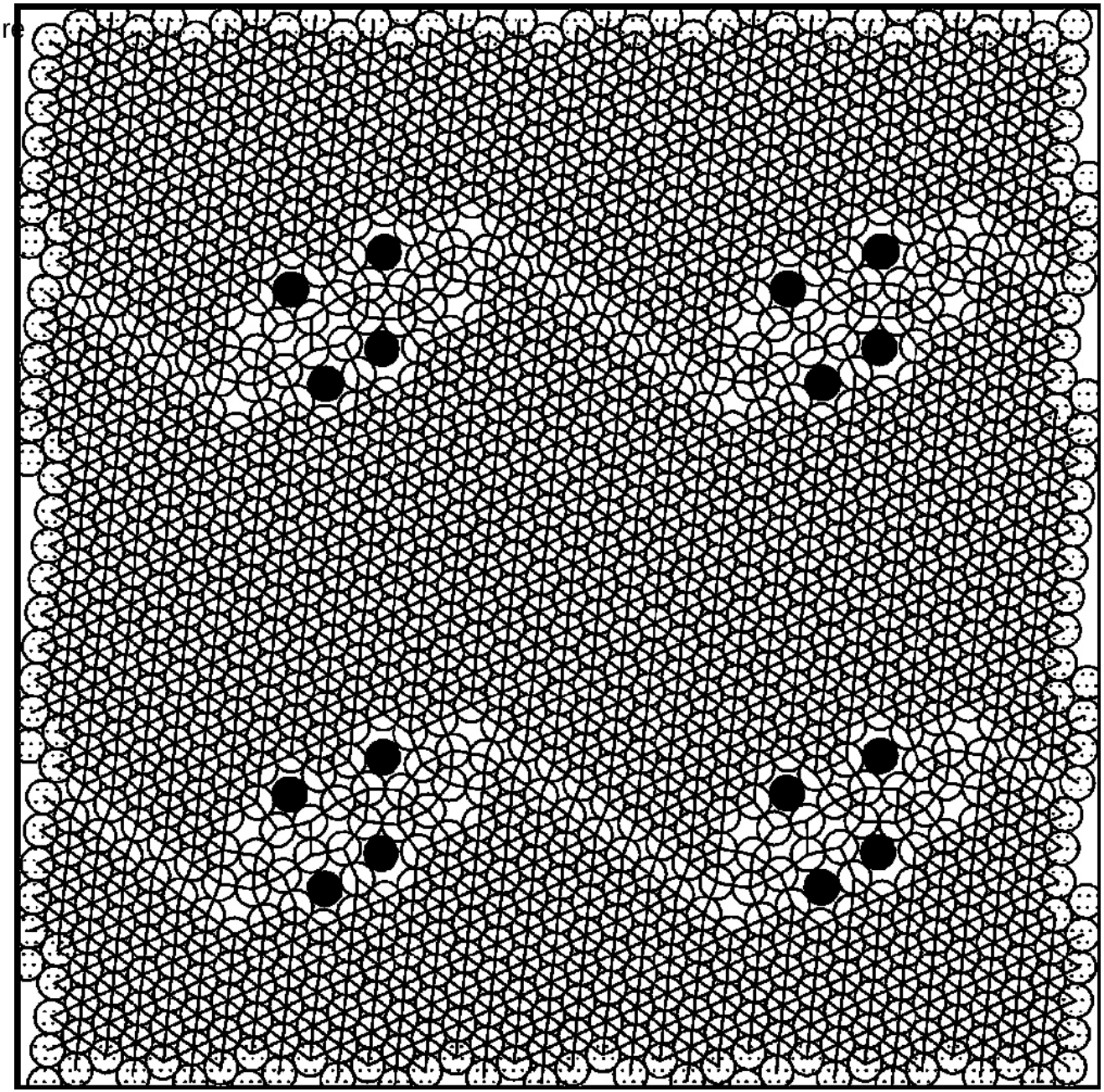

BACK

BACK

Covering Fraction Ranges, Collectively Jammed Systems

Rigid rods ($d = 1$): $\varphi \equiv \varphi_{\max}$.

Rigid disks ($d = 2$): $3\varphi_{\max}/4 \le \varphi \le \varphi_{\max}$.

Rigid spheres ($d = 3$): $2\varphi_{\max}/3 \le \varphi \le \varphi_{\max}$.

BACK

Collectively Trapped Region, Configuration Space Dimension (N-1)d

Hard particle trapping for fixed system centroid:

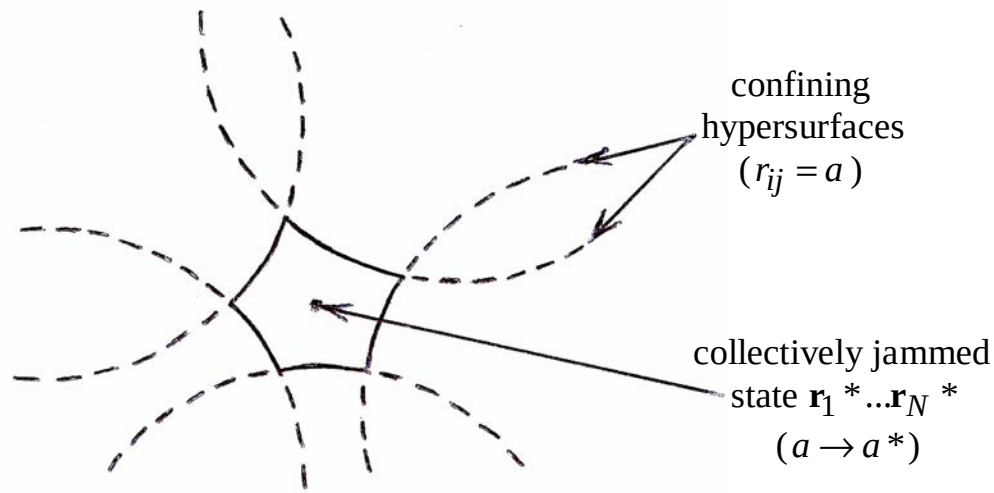

Number H of confining hypersurfaces:

Rods ($d = 1$): $H = N$,

Disks ($d = 2$): $2N - 1 \le H \le 3N$,

Spheres ($d = 3$): $3N - 2 \le H \le 6N$.

CAUTION: As a result of hypersurface curvature, strict disconnection for large N and $d \ge 2$ only occurs when $a* - a = O(N^{-1/d})$. But this involves extremely thin "filaments" with correspondingly small content.

BACK

Polytope Limit Near Jamming

- Replace bounding hypersurfaces with tangent hyperplanes:

$$r_{ij} = a \quad \rightarrow \quad (\mathbf{r}_{ij}{}^{*} \cdot \mathbf{r}_{ij}) / a^{*} = a \ .$$

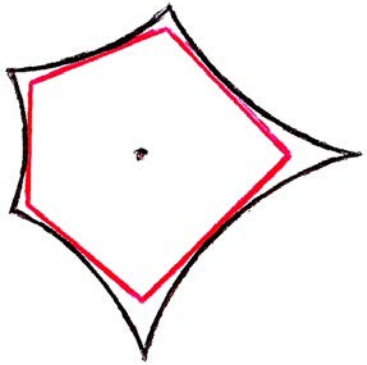

- Distances in resulting convex polytope scale as $a^{*} - a$.

- Content of polytope: $\Omega = C(a^{*} - a)^{(N-1)d}$, $C > 0$.

- Pressure equation of state (from configuration-restricted partition function):

$$\frac{p}{\rho k_B T} = \frac{d(1 - N^{-1})}{(a^{*}/a)^{d} - 1} + O(1) \ .$$

Inclusion of "rattlers" would only contribute to $O(1)$.

Some Relevant Literature

BACK

Pioneering investigation:

"Equation of State of Classical Hard Spheres at High Density", Z.W. Salsburg and W.W. Wood, J. Chem. Phys. **37**, 798 (1962).

General mathematical text, properties of polytopes:

"Convex Polytopes", B. Grünbaum, Wiley-Interscience, New York, 1967.

Hard-particle statistical mechanics papers:

"Limiting Polytope Geometry for Rigid Rods, Disks, and Spheres", F.H. Stillinger and Z.W. Salsburg, J. Stat. Phys. **1**, 179 (1969).

"Jamming in Hard Sphere and Disk Packings", A. Donev, S. Torquato, F.H. Stillinger, and R. Connelly, J. Appl. Phys. **95**, 989 (2004).

"Pair Correlation Function Characteristics of Nearly Jammed Disordered and Ordered Hard-Sphere Packings", A. Donev, S. Torquato, and F.H. Stillinger, Phys. Rev. E **71**, 011105 (2005).

Euler's Theorem

BACK

- Familiar form in $d = 3$ for any polyhedron (Euler, 1752):

$$f - e + v = 2$$

connecting numbers of faces *f*, edges *e*, and vertices *v*.

- For any polytope let f_j denote the number of its *j*-dimensional "*j*-faces".

Generalization of Euler's theorem for any $D \geq 1$ (Schläfli, 1901):

$$\sum_{j=0}^{D-1} (-1)^j f_j = 1 - (-1)^D \ .$$

- *j*-face enumeration for simplices in *D* dimensions:

$$f_j = \frac{(D+1)!}{(j+1)!(D-j)!} \ .$$

Princeton Lecture
April 12, 2007
F.H. Stillinger
Figure 11

BACK

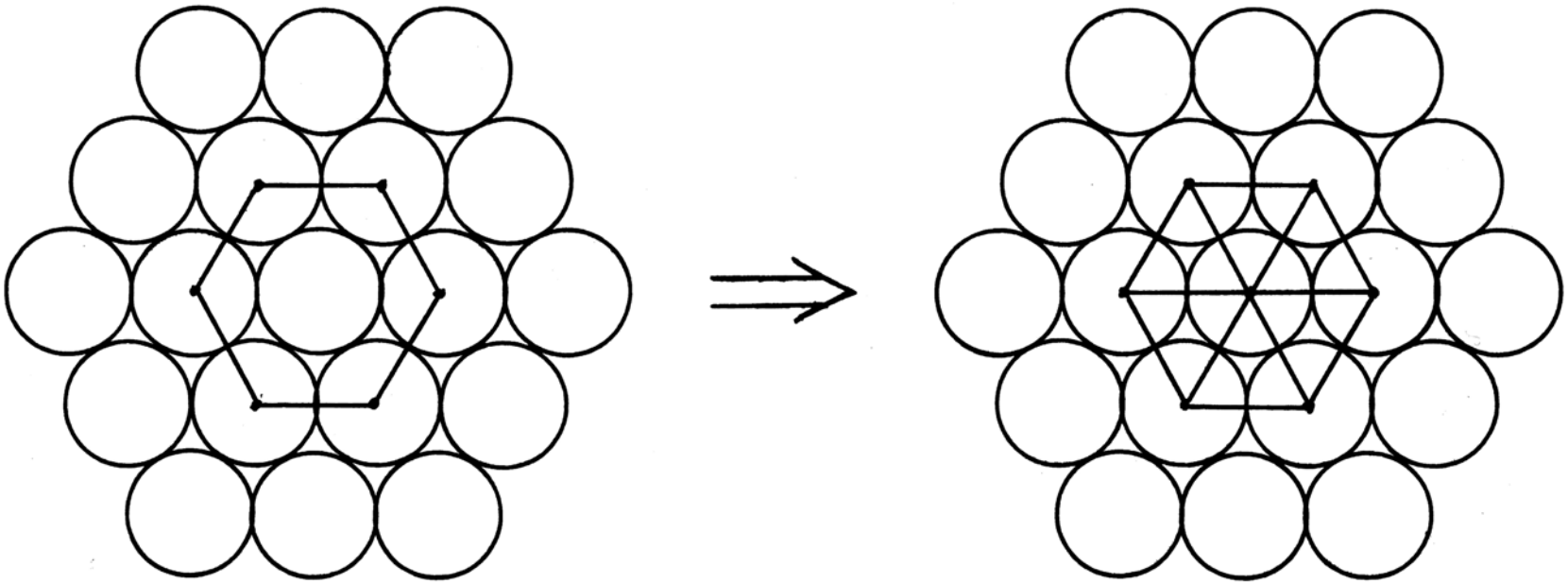

BACK

Rigid Rod System: Regular Simplex in Arbitrary Dimension

- For N rigid rods of length a on line length L, the content Ω of the fixed-centroid simplex in $N-1$ dimensions is:

$$\Omega = \frac{N^N (a^* - a)^N}{N^{1/2} N! L} \ , \qquad N^{-1} \ln \Omega \sim \ln(a^* - a) + e \ .$$

- Inscribed and circumscribed hyperspheres yield thermodynamically useless lower and upper bounds:

$$N^{-1} \ln \Omega_{in} \sim \ln(a^* - a) + (1/2) \ln(e\pi / N) \ ,$$
$$N^{-1} \ln \Omega_{circ} \sim \ln(a^* - a) + \ln\left[(e\pi / 24)^{1/2} N \right] .$$

- Independent cell approximation (enclosed hypercube) is a thermodynamically relevant, but crude lower bound:

$$N^{-1} \ln \Omega_{cell} \sim \ln(a^* - a) \ .$$

BACK

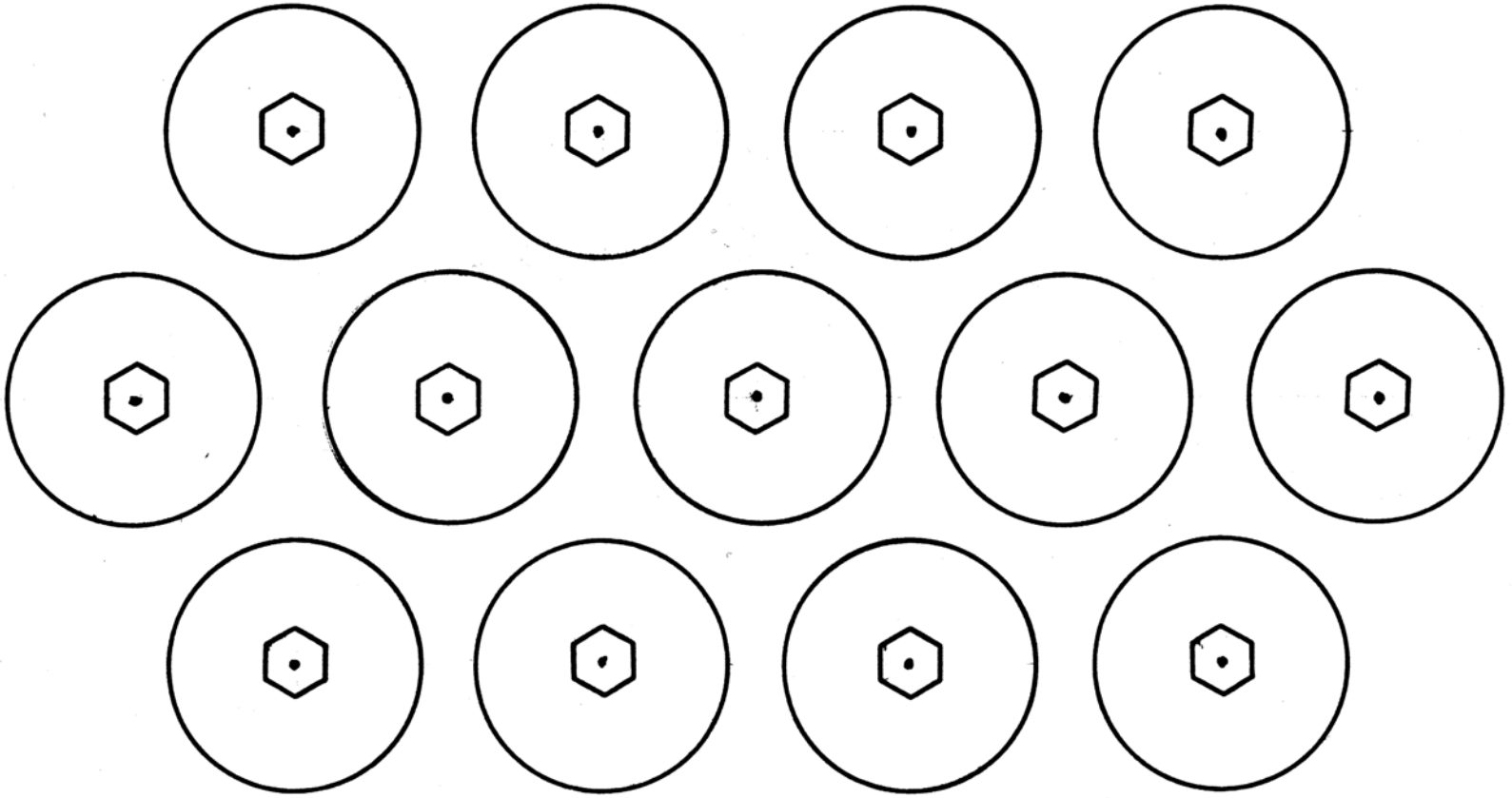

Particle-Pair Distance Distributions

BACK

- Separation probability for a contacting pair i,j is proportional to the $(D-1)$-dimensional polytope cross section $A_{ij}(r_{ij})$ swept out parallel to the i,j hyperface:

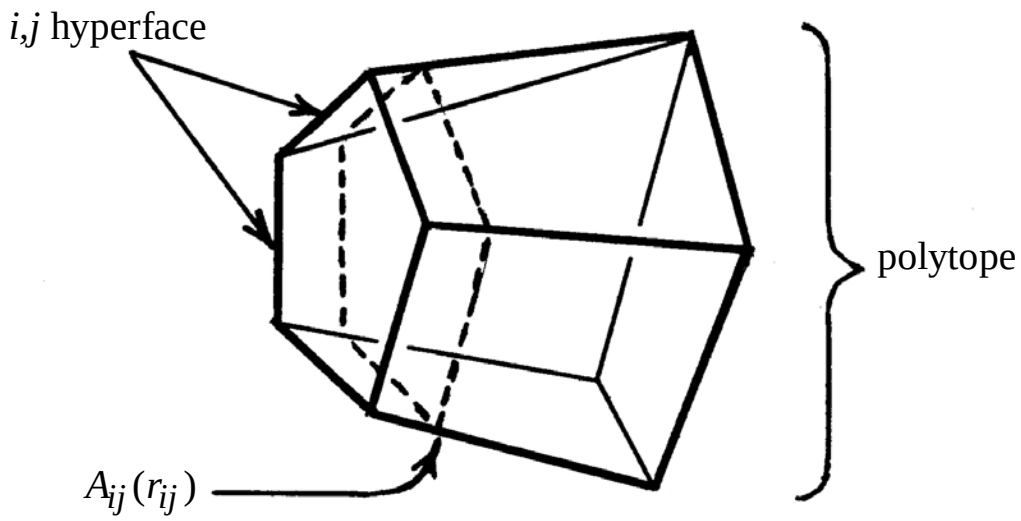

- The probability $A_{ij}(r_{ij})/\Omega$ rises discontinuously from 0 at $r_{ij} = a$.

- For non-contacting pairs k,l the cross-sectioning hyperplane also moves across the polytope by parallel displacement, but not parallel to a hyperface.
  $\Rightarrow$ No initial discontinuity.

- Conventional particle pair distribution function averages over all pairs.

BACK

Jamming Limit Scale Change

- Particle deviation from collectively jammed configuration (fixed centroid):

$$\delta\mathbf{r}_i = \mathbf{r}_i\,^* - \mathbf{r}_i \qquad (1 \le i \le N)\ .$$

- Distance scaling by collision diameter decrement:

$$\mathbf{t}_i = \delta\mathbf{r}_i\,/(a^* - a)\ .$$

- Polytope defined by scaled inequalities:

$$1 + \mathbf{w}_{ij}\cdot(\mathbf{t}_j - \mathbf{t}_i) \ge 0 \qquad (\mathbf{w}_{ij} = \mathbf{r}_{ij}\,^*/|\mathbf{r}_{ij}^*|)\ .$$

- Pair distance distributions remain well-defined as $a \to a^*$, *e.g.* for contacting neighbors:

BACK

Brünn-Minkowski Theorem

** Let $\mathbf{B}_1$ and $\mathbf{B}_2$ be two closed, bounded, convex sets in R^M, and set:

$$\mathbf{B}(\lambda) = (1-\lambda)\mathbf{B}_1 + \lambda\mathbf{B}_2 \qquad (0 \le \lambda \le 1) .$$

If $V_M(...)$ represents M-dimensional volume (content), then $\{V_M[\mathbf{B}(\lambda)]\}^{1/M}$ is a concave function of λ:

$$\{V_M[\mathbf{B}(\lambda)]\}^{1/M} \ge (1-\lambda)[V_M(\mathbf{B}_1)]^{1/M} + \lambda[V_M(\mathbf{B}_2)]^{1/M} .$$

** Application to single-pair distance distributions:
Choose $\mathbf{B}_1, \mathbf{B}_2$ to be two parallel polytope cross-sections A_{ij} for pair i,j.

With large $M = (N-1)d - 1$ the quantity $\{V_M[A_{ij}(\lambda)]\}^{1/M}$ is uninformative.

However Brünn-Minkowski concavity implies that the pair distance distribution $A_{ij}(t_{ij})/\Omega$ has no relative minima.

Contacting-Pair Distance Distribution for a Simplex

BACK

- The collective-trapping polytope is a simplex for rigid rods ($d=1$), as well as for irregular disk ($d=2$) or sphere ($d=3$) packings. These irregular packings are often labeled "isostatic".

- The cross-sectional hyper-area $A_{ij}(t_{ij})$ for a contact pair retains fixed shape as it sweeps across the simplex toward the far vertex (f_0), but its content scales downward according to a power equal to dimension $D-1=(N-1)d-1$.

- Large-N behavior of rigid-rod contact-pair distance distribution:

$$A(t)/\Omega = (const.)\times\left[1-\frac{t}{N-1}\right]^{N-2}$$

$$\sim \exp(-t) \quad .$$

- Large-N behavior of the $A_{ij}(t_{ij})/\Omega$ for irregular disk and sphere packings are also simple exponential decays, but with i,j-dependent decay rates.

BACK

Amorphous Disk and Sphere Packings

- Mean contact number for disks is 4, for spheres is 6.
- The simplectic polytopes have little or no symmetry; the hyperfaces for contact pairs have a distribution of contents $A_{ij}(1)$.
- Travel distance across simplex for cross-section $A_{ij}(t_{ij})$ is inversely proportional to $A_{ij}(1)$. $\Longrightarrow$ Exponential decay rate for distance distribution is proportional to $A_{ij}(1)$.
- Average distance distribution for contact pairs remains monotonically decreasing with distance.

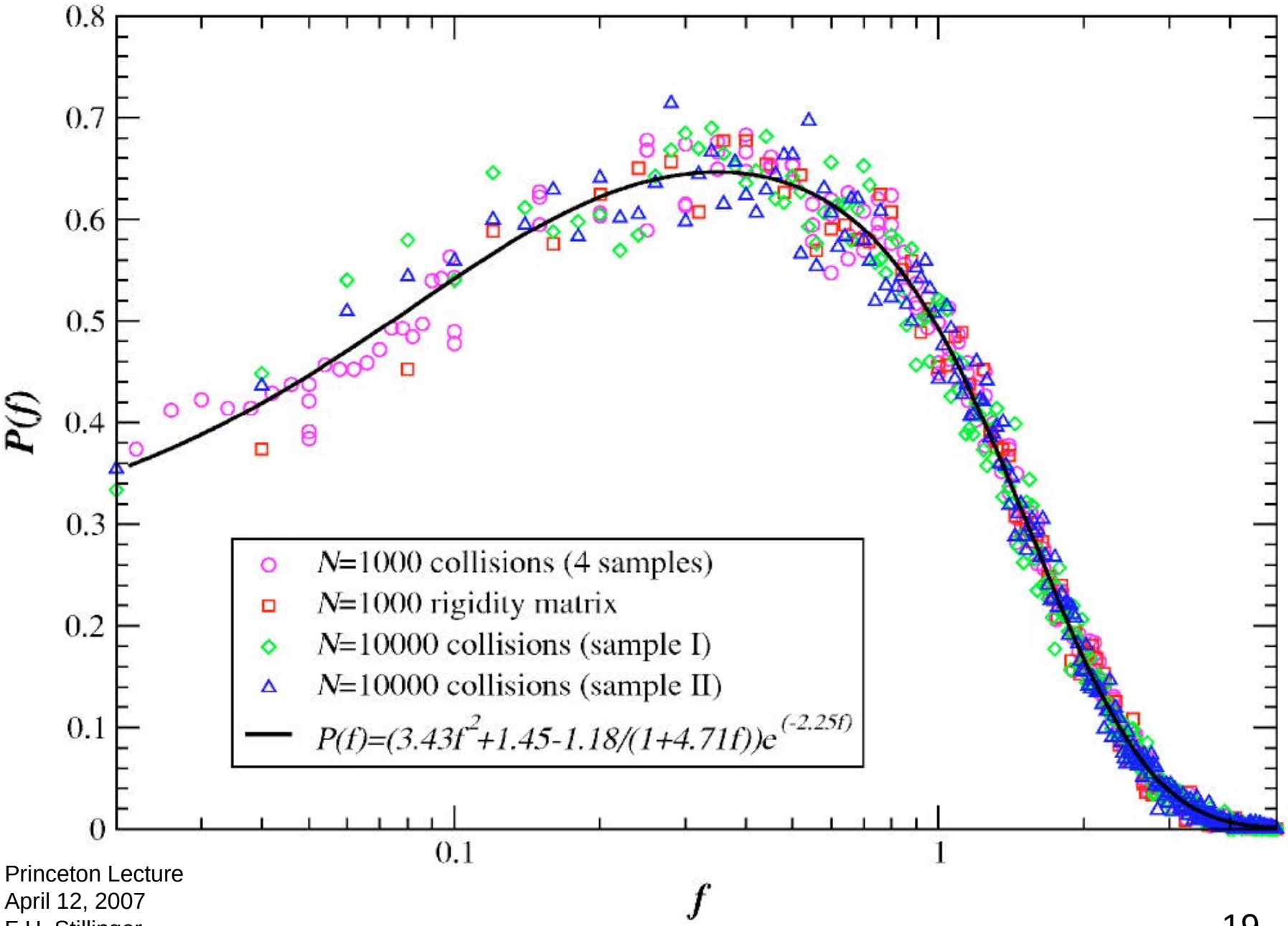

Princeton Lecture
April 12, 2007
F.H. Stillinger
Figure 19

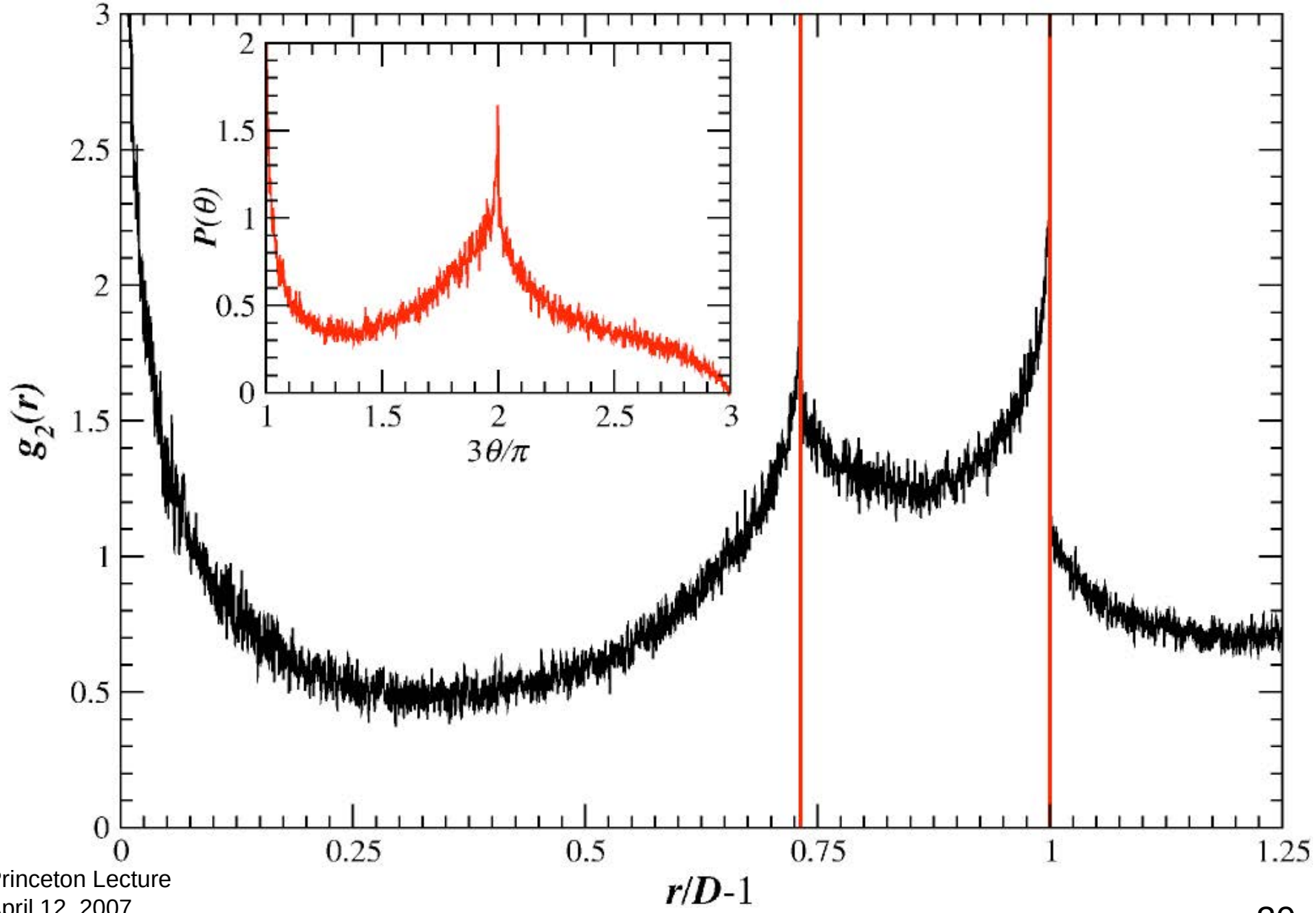

Princeton Lecture
April 12, 2007
F.H. Stillinger
Figure 20

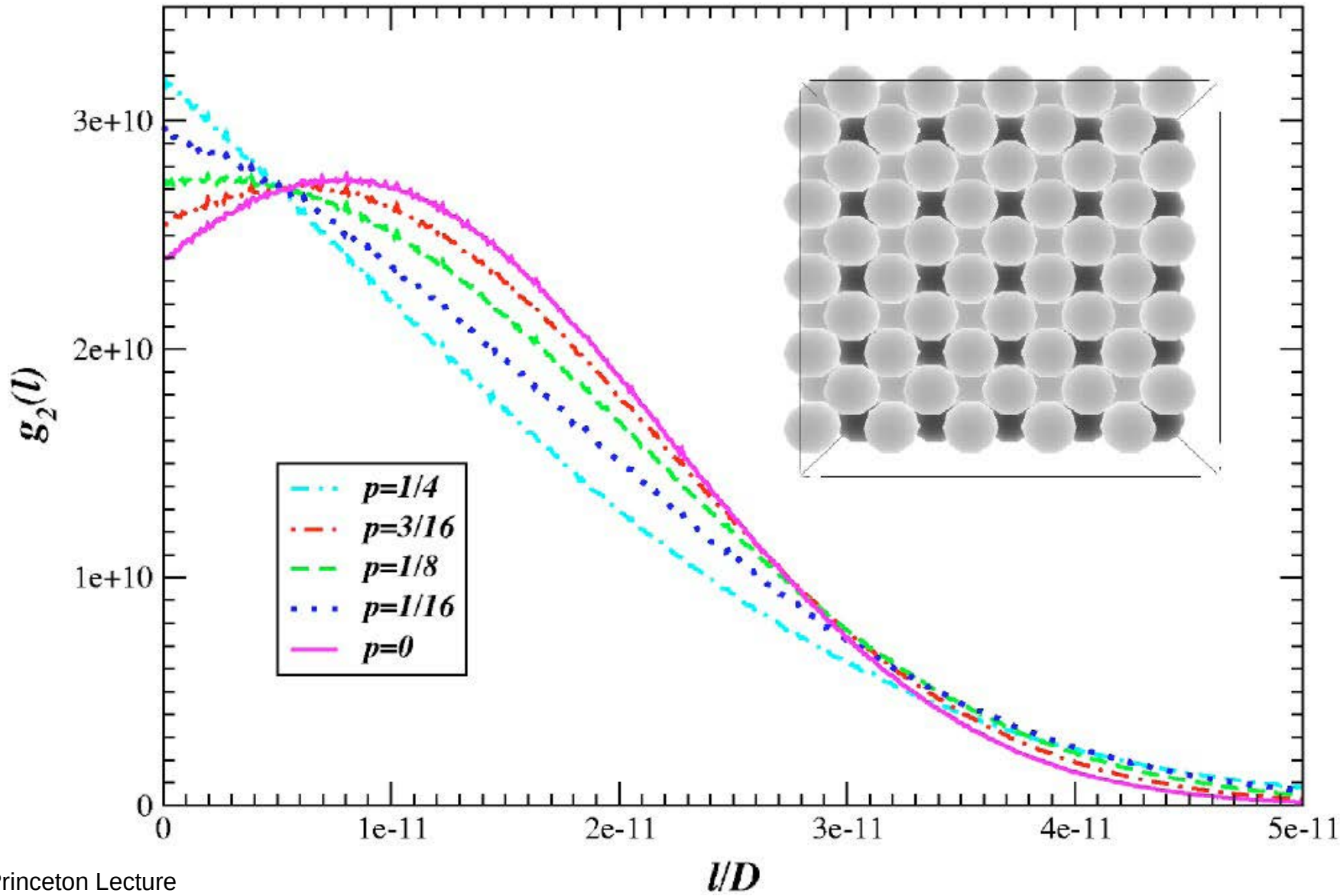
3e+10
2e+10
1e+10
0
$g_2(l)$
0
1e-11
2e-11
3e-11
4e-11
5e-11
l/D
p=1/4
p=3/16
p=1/8
p=1/16
p=0

BACK

Polytope Moment Tensor

- The polytope incenter $\mathbf{r}_1 * ... \mathbf{r}_N *$ in general will not coincide with its centroid ("center of mass").

- Restrict attention to cases of incenter-centroid coincidence:
  Particle arrangements with center of symmetry.

- $\mathbf{t} \equiv \mathbf{t}_1 \oplus \mathbf{t}_2 \oplus .... \oplus \mathbf{t}_N$

- Polytope moment tensor defined as thermal average at fixed centroid:
  $$\mathbf{T} = \langle \mathbf{tt} \rangle_{c.o.m.}$$

- Eigenvalues of $\mathbf{T}$ will yield polytope's principle moments of inertia.

BACK

Elastic Constants

- Nearly jammed triangular crystals ($d = 2$) have two isothermal elastic constants; nearly jammed FCC crystals ($d = 3$) have three isothermal elastic constants. In the high compression limit these all scale as $k_B T/(a^* - a)^2$.

- Eigenvectors of the moment tensor $\mathbf{T}$ for these perfect crystals have running-wave character (wavevector $\mathbf{k}$). Probability distributions of eigenvector amplitudes are determined by appropriately oriented polytope cross sections.

- Large-system, small-$|\mathbf{k}|$, limits for amplitude distributions determine isothermal elastic constants.

- Adiabatic elastic constants can be trivially obtained from isothermal versions for hard-particle models.

Some (of Many!) Unsolved Problems

BACK

- What collectively jammed structure(s) can host the highest rattler density?
- How is polytope geometry related to thermal conductivity?
- What is the range of covering fraction for collectively jammed hyperspheres in dimensions $d \geq 4$? Does the lower limit become an arbitrarily small fraction of $\varphi_{\max}$ as d increases?
- After creating an unstable divacancy in a perfect triangular crystal of disks, how does re-jamming influence φ and the mean contact number? Analogous question exists for a compact trivacancy in an fcc crystal.
- Starting with a jammed structurally-perfect crystal of N disks or spheres, does insertion of particle $N+1$ require an unbounded system size increase in the large-N limit?